Oral Presentation

The 7th TSME International Conference on Mechanical Engineering
13-16 December 2016

TSME ICOME 2016
Mechanical Engineering Innovation for Green Society

TSF0018

Vortex Structure around a Heaving Elastic Airfoil in Separation Region

Masaki Fuchiwaki[1*], Aphaiwong Junchangpood[2], and Kazuhiro Tanaka[1,]

[1] Kyushu Institute of Technology, 680-4 Kawazu, Iizuka, 8208502, Japan
[2] King Mongkut's University of North Bangkok, 1518 Pibulsongkram Road Bangsue, Bangkok, 10800, Thailand
[*] Corresponding Author: futiwaki@mse.kyutech.ac.jp, +81-0948297763, +81-0948297751

Abstract

Many researchers have experimentally and numerically investigated the flow field around an unsteady airfoil, which is a common unsteady flow. In recent years, the flow field in the vicinity of moving airfoils capable of flexible elastic deformation has become a focus of attention, and its effects are beginning to be understood. Flow in the vicinity of an elastically deforming airfoil may be understood as a fluid-structure interaction (FSI) problem, and the motion and deformation of elastic airfoils, as well as the associated vortex flow phenomena in their vicinity, are complicated. In this study, the dynamic behavior of the vortices rolled up from the leading edge of a heaving elastic airfoil in a separation region through FSI simulation using ANSYS 16.1/ANSYS CFX 16.1. The vorticity of the leading edge vortex on the heaving elastic airfoil was higher than that on the rigid airfoil, and the growth of the leading edge vortex on the elastic airfoil is slightly delayed in comparison with that on the rigid airfoil because the effective angle of attack of the elastic airfoil is smaller than that of the rigid airfoil. Moreover, the micro scale vortices on the suction surface interfere with the leading-edge vortex. As a result, the rotation of the leading-edge vortex is strengthened, and its growth is delayed.

Keywords: Airfoil, Vortex, Separation, Fluid structure Interaction.

1. Introduction

The flow field around an unsteady airfoil is a common type of unsteady flow, and many researchers have experimentally and numerically investigated unsteady flows around moving airfoils. Previous studies have reported on not only the dynamic behavior of vortices rolled up from the leading and trailing edges of moving airfoils, such as a pitching airfoil, a heaving airfoil, and a combination airfoil with pitching and heaving motions, but also their dynamic lift and thrust characteristics [1]-[5]. Fuchiwaki et al. reported that the leading edge vortex of a pitching airfoil at an angle of attack of 16 deg., which is in a separation region under stationary conditions, reattached on the suction surface [6], this reattachment contributed to the dynamic lift acting on the pitching airfoil [7]. Maresca et al also reported the reattachment of the leading edge vortex in a heaving airfoil [8].

In recent years, the flow field around moving airfoils capable of flexible elastic deformation, such as the wings of flying insects or the tail fins of water-based organisms swimming through fluids, has become a focus of attention, and the effects of such flow fields are beginning to be understood [9]-[14]. The flow field around an elastically deforming airfoil may be understood as a fluid-structure interaction (FSI) problem, and the motion and deformation of elastic airfoils, as well as the associated dynamic behavior of the vortices, are complicated.

The flow field around an elastic body has been investigated primarily through experimental studies. Fuchiwaki et al. [15] applied a heaving motion to a moving elastic airfoil and studied the vortex structure of the wake and the nature of the dynamic thrust acting on the airfoil. Kurinami et al. [16] reported that the dynamic thrust acting on a heaving airfoil depends strongly on the Strouhal number, which is proportional to the maximum amplitude at the trailing edge of the airfoil. Heathcote et al. [17] reported the trailing edge of a heaving airfoil that deforms elastically and clarified the effect of chordwise flexibility on the dynamic thrust based on the results of particle image velocimetry (PIV) measurement and dynamic thrust measurements. Heathcote et al. [18] also clarified the relationship between the flow pattern in the wake and the dynamic thrust characteristics through the results of PIV measurement and dynamic thrust measurements of an elastic airfoil with spanwise flexibility. Gordnier et al. [19] clarified the effects of the angle of attack and the Reynolds number on the flow field by varying the oscillation of a thin elastic plate at low Reynolds numbers. They reported that the oscillation of a thin elastic plate causes the stall angle to change and reduces the Reynolds shear-stress. Furthermore, the relationship between the elastic deformation and the flow field was surveyed. Young et al. [20] experimentally and numerically demonstrated that the elastic deformation of the blade of a marine propeller can reduce the vibration and noise without reducing the propeller efficiency.

In this study, the dynamic behavior of the vortices rolled up from the leading edge of a heaving elastic airfoil in a separation region through FSI simulation using ANSYS 16.1/ANSYS CFX 16.1. In particular, the FSI simulation of the flow field on a heaving elastic airfoil at an angle of attack of 16°, which is in the separation region under stationary conditions, and the dynamic behavior of both the leading edge vortex

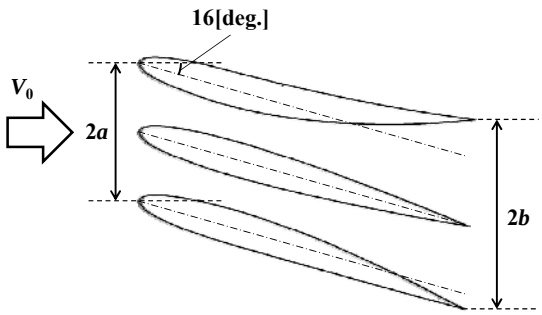

Fig. 1 Airfoil configuration and its elastic deformation in our fluid structure interaction simulation

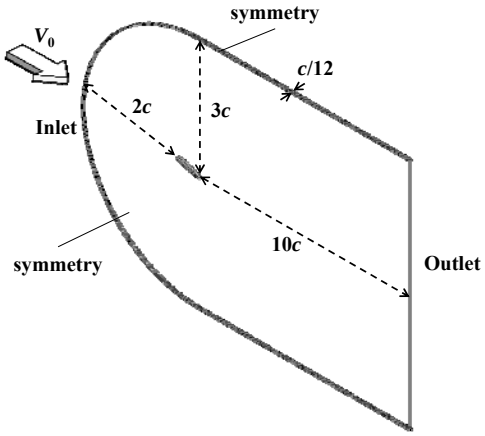

Fig. 2 Computational domain for our fluid structure interaction simulation using ANSYS16.1 and ANSYS-CFX16.1

and the vorticity in the vicinity of the suction surface were clarified.

2. Numerical simulation

2.1 Airfoil model

The elastic airfoil used in our simulation is a NACA0010 airfoil, as shown in Fig. 1. The chord length c of the airfoil is 60 [mm]. Based on this chord length, the Reynolds number is 4,000. The elastic NACA0010 airfoil consists of a rigid part and an elastic part. The ratio of the length of the rigid and elastic parts is 1:1.The heaving motion of Eq. (1) was applied to the quarter chord axis of the airfoil. The Strouhal number is given by Eq. (2) as a function of the maximum trailing edge amplitude and was 0.3 in this study. The flapping frequency, f, was 0.833 [Hz], the main flow velocity, V_0, was 0.067 [m/s] and the heaving amplitude, a, was 12 [mm] and means 0.2c.

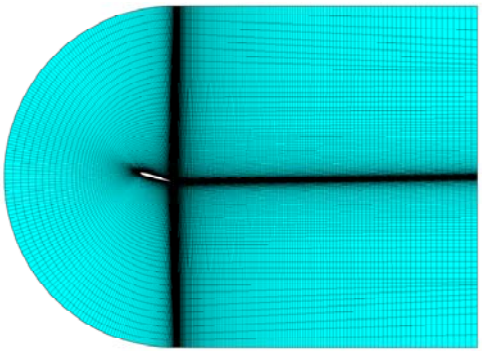

(a) Overall

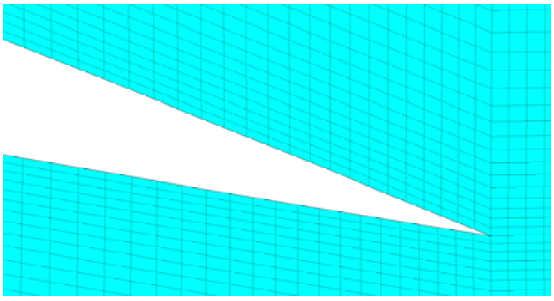

(b) Around trailing edge

Fig. 3 Computational grid around an elastic heaving airfoil

Moreover, the bending stiffness K is defined by Eq. (3) and it is considered by the second moment of area I_G, the Young's modulus E, the density ρ, and the area of the airfoil A.

$$y = a\sin(2\pi ft) \quad (1)$$

$$St = \frac{2af}{V_0} \quad (2)$$

$$k = \frac{EI_G}{0.5\rho V_0^{\,2} Ac^2} \quad (3)$$

2.2 Numerical method

In the present study, the flow field around the heaving elastic airfoil was numerically simulated through a fluid structure coupled analysis using ANSYS16.1 and ANSYS-CFX16.1. For the fluid, the governing equations are the continuity and the Navier-Stokes equations given by Eqs. (4) and (5), respectively, and the finite volume method (FVM) was used for discretization. For the structural part, the governing equations are the constitutive equations given by Eq. (6), and the finite element method (FEM) was used for discretization.

As shown in Fig. 2, the vertical length of the leading edge, trailing edge, and airfoil surface in the analysis region are defined with respect to the chord length c as $2c$, $10c$ and $3c$. Additionally, the spanwise depth of the airfoil was set to $c/12$. Figure 3(a) and (b)

Table 1 Computational conditions on fluid part

Fluid	Water
Inlet	Constant velocity
Outlet	Constant pressure
Wall	Symmetry
Turbulence	*k-ω*
y^+	$y^+ < 5$
Nodes	280,000
Mesh	Hexa
Time step *t*	0.01 [s]
Total time	10×*T*

Table 2 Computational conditions on structure part

Strucuture	Silicone
Hyperelastci model	Neo-Hookean
Young's modulus	0.06 [MPa]
Poisson ratio	0.45
Density	1143 [kg/m^3]
Nodes	5,000
Mesh	Hexa
Time step *t*	0.01 [s]
Total time	10×*T*

shows the overall numerical mesh and an enlarged view of the mesh around the trailing edge, respectively. The numbers of cells in the computational grids for the fluid and structure regions are 280,000 and 5,000, respectively. The height of the first lattice point is approximately 0.002 of the chord length *c*. A boundary-surface transmitting pressure and displacement data were defined at the airfoil surface. The numerical conditions of the fluid and structure regions are given in Tables 1 and 2.

$$\nabla \bullet U = 0 \quad (4)$$

$$\rho \frac{\partial U}{\partial t} + (U \bullet \nabla)U = -\nabla P + \mu \nabla^2 U \quad (5)$$

$$[M]\ddot{X} + [C]\dot{X} + [K]X = F \quad (6)$$

3. Results and discussion

3.1 Dynamic behavior of leading edge vortex

Figure 4(a) and (b) shows the vorticity distributions around the leading edge of the heaving rigid and elastic airfoils during one heaving cycle, respectively. The blue and red in Fig. 4 indicate vorticity rotation in the clockwise and

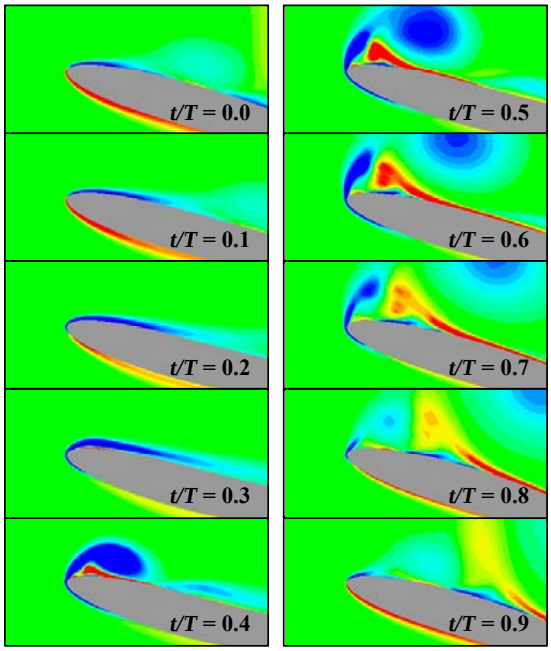

(a) Rigid airfoil

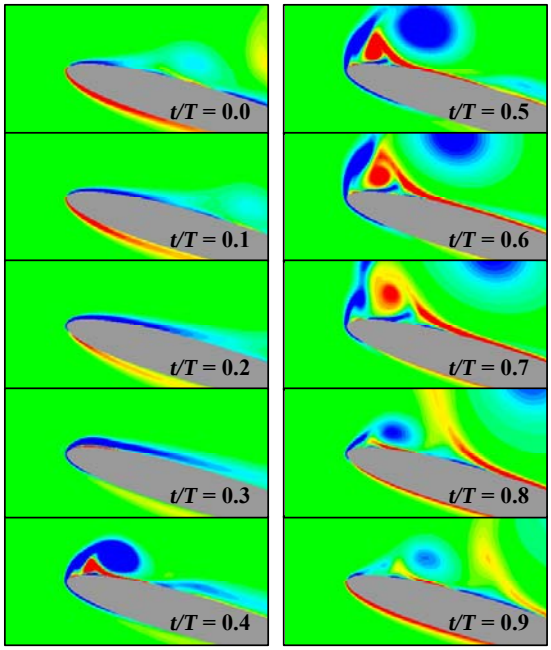

(b) Elastic airfoil

Fig. 4 Vorticity distribution around a leading edge of heaving airfoils

counterclockwise directions, respectively. t/T = 0.0 and 0.5 correspond to the centers of the heaving motion from the bottom dead position to the top dead position and from the top dead position to the bottom dead position.

The dynamic behavior of the leading-edge vortex in both airfoils was almost the same from the top dead position (t/T = 0.0) to the bottom dead position (t/T =

0.5), and the leading-edge vortex reattaches on the suction surface. A previous study by the present authors reported that the leading-edge vortex of a pitching rigid airfoil in the separation region at an angle of attack of 16° and a high Strouhal number reattached on the suction surface and that the separation was controlled under these conditions [6][7]. Maresca et al. [8] have reported that the heaving rigid airfoil exhibited the same dynamic behavior as the pitching rigid airfoil. These results indicate that the separation on the heaving elastic airfoil may be controlled by the leading-edge vortex rolled up from the elastic airfoil. As the airfoil moves away from the bottom dead position, the leading-edge vortex separates from the suction surface; however, the growth of the leading-edge vortex on the elastic airfoil is slightly delayed in comparison with that on the rigid airfoil. Moreover, the maximum vorticity of the leading-edge vortex on the elastic airfoil at the bottom dead position was –170.74 [s^{-1}] and was larger than that of the rigid airfoil, which was –120.45 [s^{-1}]. These phenomena are due to the small effective angle of attack, α_{eff}, of the elastic airfoil. The effective angles of attack of the rigid and elastic airfoils are defined in Eqs. (7) and (8) [17], respectively, and the effective angle of attack of the elastic airfoil is reduced by the elastic deformation of the trailing edge, which is not symmetric, as shown in Fig. 1, because of the angle of attack of 16°, and is thus maximized at t/T = 0.5. The maximum effective angle of attack of the elastic airfoil is 48.8°, which is approximately 20% less than that of the rigid airfoil. These results indicate that the small effective angle of attack on the elastic airfoil contributes to not only the strengthening of the leading-edge vortex but also the delay in its growth.

$$\alpha_{eff} = \tan^{-1}\left(\frac{-V_{LE}}{V_0}\right) - \varphi \qquad (7)$$

$$\alpha_{eff} = \tan^{-1}\left(\frac{-V_{LE}}{V_0}\right) - \alpha_{ela} - \varphi \qquad (8)$$

3.2 Micro scale vortices on the suction surface

As shown in Fig. 4, the vorticity with counterclockwise rotation (red) was observed below the leading edge vortex with clockwise rotation (blue) on both airfoils, and the region of this vorticity on the elastic airfoil was slightly larger than that on the rigid airfoil. These vorticities result in the growth of micro scale vortices on the suction surface. Next, these micro scale vortices were evaluated quantitatively, and the vorticities ω_z on the suction surfaces of both airfoils were measured. The vorticities ω_z were calculated using the FSI simulation and were obtained from the second grid point in fluid region, as shown by the red line in Fig. 5, because the data of the first grid point contains a turbulence model correction.

Figure 6(a) and (b) shows the vorticities ω_z on the suction surfaces of the rigid and the elastic airfoils, respectively. The positive and negative values on the vertical axis represent counterclockwise and clockwise rotations, respectively. Figure 7(a) and (b) shows the pattern diagrams of the vorticities at t/T = 0.4 on the suction surface on the rigid and the elastic airfoils, which were obtained based on Fig. 6(a) and (b), respectively. The blue and red in Fig. 7 represent the clockwise and counterclockwise rotation of the vorticity, respectively.

In both airfoils, a strong positive peak in the

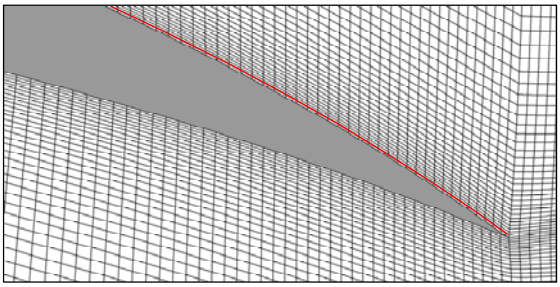

Fig. 5 Measurement point of vorticities, ω_z, from second grid point

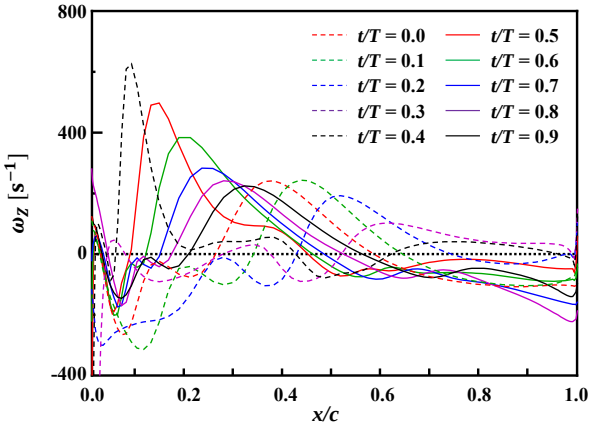

(a) Rigid airfoil

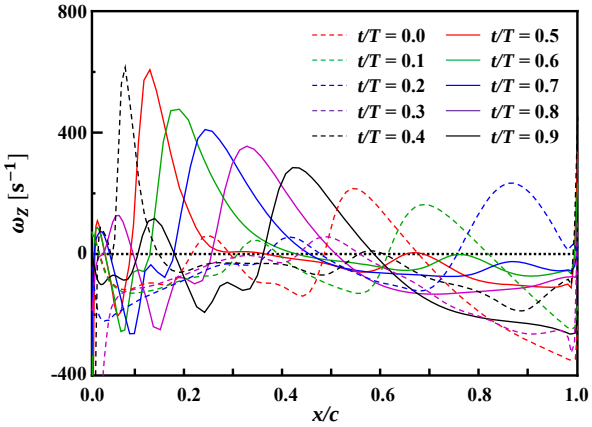

(b) Elastic airfoil

Fig. 6 Vorticity distributions on second grid point in heaving airfoils

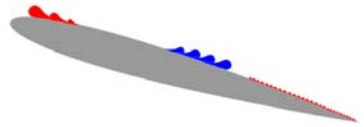

(a) Rigid airfoil

(b) Elastic airfoil

Fig. 7 Pattern diagrams of vortices on the suction surface in the heaving airfoils based on Figs. 6

vorticity was observed on the suction surface at t/T = 0.4, indicating the presence of micro scale vortices with counter clockwise rotation below the leading edge vortex, as shown in Fig. 6. Furthermore, in Fig. 7, the vortices with counter clockwise rotation near the leading edge can be visually observed. These vorticities were predisposed to decreasing over time. In the elastic airfoil, all vorticities decreased at the almost same rate and were higher than those on the rigid airfoil. That is, the micro scale vortices on the suction surface likely interfered with the leading edge vortex, resulting in the strengthening of the rotation of the leading-edge vortex and the delay in its growth. After that, micro scale vortices developed on the suction surface until the trailing edge clearly, as shown in Fig. 6(b). On the elastic airfoil, the micro scale vortices could continue to grow because the elastic airfoil experienced elastic deformation around the trailing edge. In contrast, on the rigid airfoil, the micro scale vortices were very small, as shown in Fig. 6(a); this means that the micro scale vortices disappeared without growing on the suction surface, because the airfoil experienced no elastic deformation. This indicates that the elastic deformation contributes to the growth of micro scale vortices on the suction surface. Moreover, these micro scale vortices strongly influenced the dynamic behavior of the leading edge vortices. Based on these results, the elastic deformation of the airfoil likely plays an important role in defining the dynamic behavior of the leading-edge vortex.

4. Concluding remarks

The dynamic behavior of the leading edge vortex rolled up from a heaving elastic airfoil in the separation region at an angle of attack of 16° and the vorticity in the vicinity of the suction surface were investigated by FSI simulation using ANSYS 16.1/ANSYS CFX 16.1.

The vorticity of the leading edge vortex on the heaving elastic airfoil was higher than that on the rigid airfoil, and the growth of the leading edge vortex on the elastic airfoil is slightly delayed in comparison with that on the rigid airfoil because the effective angle of attack of the elastic airfoil is smaller than that of the rigid airfoil. Moreover, the micro scale vortices on the suction surface interfere with the leading-edge vortex. As a result, the rotation of the leading-edge vortex is strengthened, and its growth is delayed.

5. Acknowledgement

The authors are grateful to the Harada Kinen Foundation for supporting the present research.

6. References

[1] Garrik, I. E. (1936). Propulsion of a flapping and oscillating airfoil, *NACA Report,* No.567, pp. 419-427.
[2] Jones, K.D., Dohring, C.M., and Platzer, M.F. (1998). An Experimental and Computational Investigation of the Knoller-Betz Effect, *AIAA Journal*, Vol.36(7), 1240-1246.
[3] Lai, J.C.S., Platzer, M.F. (1999). Jet Characteristics of a Plunging Airfoi, *AIAA Journal*, Vol.37(12), pp. 1529-1537.
[4] Ramamurti, R., and Sandberg, W. (2001). Simulation of Flow About Flapping Airfoils Using Finite Element, *Journal of Experimental Biology*, Vol.210, pp. 881-896.
[5] Fuchiwaki, M., and Tanaka, K. Two-dimensional structure of the wake behind a pitching airfoil with higher non-dimensional pitching rate, *Journal of Visualization*, Vol.4(4), pp. 323-329.
[6] Fuchiwaki M., and Tanaka K. (2000) Arrangement and Dynamic Behavior of Vortices from a Pitching Airfoil, *JSME international journal. Ser. B, Fluids and thermal engineering*, Vol.43(3), pp.443-448.
[7] Fuchiwaki M., Tanaka K., and Tanaka H. (1999) Unsteady Characteristics of Lift and Drag Acting on a Pitching Airfoil, Transactions of the Japan Society of Mechanical Engineers, Series B, Vol.65(634), pp.1970–1977 (in Japanese).
[8] Maresca, C., Favier, D., and Rebont, J., (1979) Experiments on an aerofoil at high angle of incidence in longitudinal oscillations, Journal of Fluid Mechanics, Vol. 92 (4), pp. 671-690
[9] Fuchiwaki M., Kurinami T., Nagata T., Tanaka K., and Tabata T. (2010) Vortex Structure around Moving Elastic Airfoils and Their Characteristics of Dynamic Forces, paper presented in *the ASME 2010 3rd Joint US-European Fluids Engineering Summer Meeting*, Montreal, Canada.
[10] Hover, F.S., Haugsdal, O., and Triantafyllou, M.S. (2004). Effect of angle of attack profiles in flapping foil propulsion", *Journal of Fluid and Structure*, Vo.19, pp. 37-47.
[11] Tang, J., Viieru D. and Shyy W., (2007), A study of aerodynamics of low Reynolds number flexible

airfoils, *37th AIAA Fluid Dynamics Conference and Exhibit* 25-28 June(2007), Miami, FL, 4212.

[12] Murray M. M., (2000), Hydroelasticity modeling of flexible propulsors, Ph.D. Dissertation, Duke University, Durham, NC.

[13] Erath, W., Wotny, B., and Maetz, J. (1999). Modeling the fluid structure interaction produced by a waterhammer during shutdown of high-pressure pumps, *Nuclear Engineering and Design*, Vol.193, pp.283-296.

[14] Maio, J. M., and Ho, M.H. (2006). Effect of flexure on aerodynamic propulsive efficiency of flapping flexible airfoil, *Journal of Fluid and Structures*, Vol.22, pp. 401-419.

[15] Fuchiwaki, M., Kurinami, T., and Tanaka, K. (2009). Detailed Wake Structure behind an Elastic Airfoil, *Journal of Fluid Science Technology*, Vol.4(2), pp. 391-400.

[16] Kurinami, T., Fuchiwaki, M., Tanaka K. (2011). Vortex Flow Developed in the Vicinity of a Wall of an Elastic Heaving Airfoils and its Wake Structure, *Journal of Fluid Science Technology*, Vol.6(4), pp.562-574.

[17] Heathcote, S., and Gursul, I. (2007), Flexible Flapping Airfoil Propulsion at Low Reynolds Numbers, *AIAA Journal*, Vol.45(5), pp.1067–1079.

[18] Heathcote, S., Wang, Z., and Gursul, I. (2008). Effect of spanwise flexibility on flapping wing propulsion, *Journal of Fluid and Structure*, Vol.24, pp.183–199.

[19] Gordnier, R. E., and Demasi, L., (2013), Implicit LES Simulations of a Flapping Wing in Forward Flight, Proceedings of the *.ASME 2013 Fluids Engineering Summer Meeting,* FEDSM 2013-16540.

[20] Young Y. L., (2008), Fluid–structure interaction analysis of flexible composite marine propellers, *Journal of Fluid and Structure*, Vol. 24, pp. 799-818.